ARTICLE

Zigzag Graphene Nanoribbons with Saturated Edges

Konstantin N. Kudin*

Princeton Institute for Science and Technology of Materials (PRISM), Princeton University, Princeton, New Jersey 08544

ABSTRACT Zigzag graphene nanoribbons with saturated edges are investigated by first principles calculations. In these structures edge carbons have either two H or two F atoms, and are of sp^3 type. Compared to the previously studied ribbons with all carbons of sp^2 type, several similarities and differences are found. Specifically, in narrower ribbons the closed shell electronic state is the most stable one. In wider ribbons a state with antiferromagentically spin-polarized edges is the lowest in energy, similarly to the ribbons with all sp^2 type carbons. A notable feature of narrower ribbons is significant single—double carbon bond alternation across the ribbon. Calculated Raman spectra contain a distinct blue shift signature of such alternation, which perhaps can be used for the experimental identification of ribbons of this type.

KEYWORDS: zigzag graphene nanoribbon · density functional theory calculation · spin-polarized electronic state · band gaps · band structure · vibrational frequencies · Raman intensities

Theoretical discovery of peculiar magnetic states[1−4] at the edges of zigzag graphene nanoribbons (GNRs) has sparked significant interest toward such structures. Calculations show that under external electric field the zigzag GNRs become half-metallic, suggesting possibilities for spin-polarized electron transport.[5−13] While GNRs with such spin states have not yet been studied experimentally, other devices based on GNRs have been realized, with a range of demonstrated electronic effects.[14−17] With nanoelectronics applications in mind, studies have focused on understanding electronic properties of GNRs. For the experimentally accessible GNRs it was determined that the band gap varies inversely with the width,[18] the trend that also emerged from theoretical studies of certain GNR types.[19,20] In this work we investigate ribbons where the lowest energy electronic state changes with the ribbon width, and this state switch significantly alters the band-gap behavior. These structures have emerged from the experimental and theoretical study of the graphite oxidation products.[21] Among various model systems proposed in ref 21, ribbons formed within the planes of graphene turned out to be especially interesting. Specifically, their calculated nonresonant Raman bands were found to be in good agreement with the experimental spectra of graphite oxide,[21] and thus it can be envisioned that such ribbons may be formed as intermediates upon graphite oxidation.

In the zigzag GNRs studied previously[1−7] all carbon atoms were of sp^2 type, and possessed a free p orbital that participated in the π-electron system of the ribbon. In contrast, the ribbons formed on the graphene sheet have edge carbons of sp^3 type with no free p orbitals to contribute to the π system. To the best of our knowledge, ribbons of such kind have not been discussed yet in the literature. To gauge the potential of the GNRs with the sp^3 edge carbons for possible applications, we undertook a first principles study, and report here the effects of the width and various edge terminations on GNRs' electronic and structural properties.

RESULTS AND DISCUSSION

The carbons at the edges of the zigzag GNRs are converted to the sp^3 type by attaching two hydrogens or two fluorines, and in the following we refer to such ribbons as GNR-H_2 and GNR-F_2, respectively. We employ the customary notation for the ribbon width,[1] using N to represent the number of zigzag chains of carbons. Specifically, the smallest ribbon composed of a single layer of fused benzene rings corresponds to $N = 2$ (two zigzag carbon chains). Figure 1 depicts structures for $N = 5$ and $N = 6$. For even N the sp^3 carbons on the zigzag edge are exactly aligned, while for odd N there is a half-lattice shift. To obtain the GNR width between carbons on the oppo-

*Address correspondence to kkudin@princeton.edu.

Received for review September 12, 2007 and accepted February 04, 2008.

Published online February 16, 2008.
10.1021/nn700229v CCC: $40.75

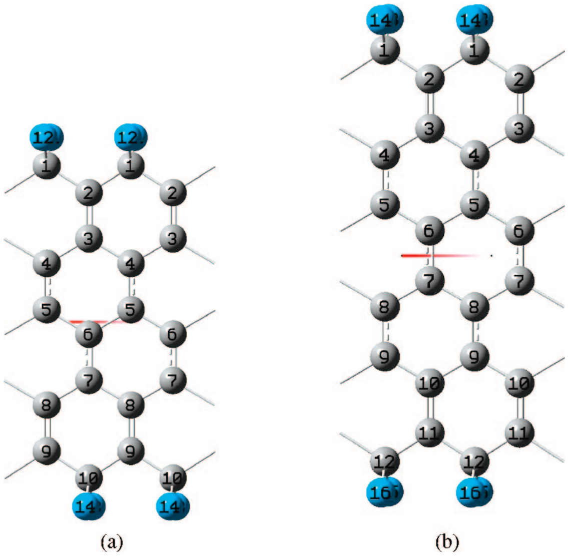

Figure 1. Ribbons with the sp^3 edge carbons for (a) $N = 5$ and (b) $N = 6$. Single, double, and conjugated bonds are drawn according to the distance criteria by GaussView[32] (double bond is between 1.248 and 1.386 Å, conjugated bond is between 1.387 and 1.447 Å, single bond is between 1.448 and 1.632 Å.)

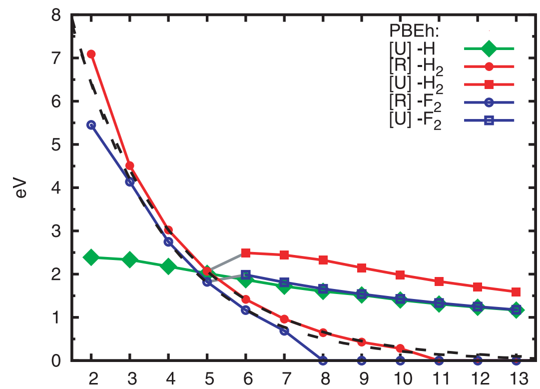

Figure 2. Band gaps for zigzag ribbons as a function of N. The following ribbon types are included: GNR-H_2, GNR-F_2, and GNR-H from ref 1 In GNR-X_2 (X = H,F) the [U] spin state first appears at $N = 6$ (indicated by the gray segments that split the respective curves into two). The exponential fits for the [R] spin state (fitted to $N = 4-6$) are shown in black dashed lines, and are described by the following expressions: gap(GNR-H_2) = $13.768e^{-0.379N}$, gap(GNR-F_2) = $14.955e^{-0.423N}$.

site zigzag edges, the following expression can be used: $W = (2.13N - 1.42)$ Å.

Calculations were carried out with the periodic boundary conditions implementation of Kudin and Scuseria.[22] For systems periodic in one dimension, this approach provides not just relative but *absolute* orbital energy levels with respect to the vacuum level. We tested both gradient corrected and hybrid density functionals:[23] PBE[24] and hybrid PBEh (aka PBE0 and PBE1PBE),[25] respectively, with the 3-21G basis set. While in spin-restricted calculations both functionals gave mostly similar results, in spin-unrestricted runs more significant differences were found. (see Supporting Information for details). Therefore, all local basis set results are reported for the PBEh functional, which is known to provide accurate estimates of band gaps for a diverse range of systems.[19,26] Moreover, from the studies of *trans*-polyacetylene[27] it is known that single−double carbon bond alternation is quite sensitive to the level of theory employed, and hybrid functionals predict bond lengths that are the closest to the experimental values among the various groups of functionals. Finally, the nonresonant Raman spectra were computed with the plane wave approach and the PBE functional, due to the unavailability of PBEh.

The band gaps for ribbons with $N = 2-13$ are given in Figure 2. In the following discussion, the spin-restricted state is labeled as [R], while the spin-unrestricted state is labeled as [U]. The specific spin-unrestricted state [U] that we focused on corresponds to the antiferromagnetic spin coupling between the ribbons' edges. This state was found to be of significantly lower energy than the ferromagnetically coupled one. All initial guesses for narrower ribbons converged to the [R] spin solution, then at $N = 6$ a stable antiferromagnetic state [U] also emerged. For the [R] state, the differences in the gap values between GNR-H_2 and GNR-F_2 become quite small for $N = 3$ and higher. Furthermore, in this state GNR-H_2 ribbons become metallic at $N = 11$, and GNR-F_2 ribbons become metallic at $N = 8$. We fitted these band gap values to the exponential expression Ae^{-BN}, and obtained good fits for both structures (see caption of Figure 2 for details). The exponential decay abruptly ends at the point where the [R] state band gap becomes zero. In contrast, the [U] state gives significantly larger gaps than the [R] state for the same width N, and the [U] band gap exhibits a much slower decay with N. The range of ribbons investigated here in the [U] state did not allow for a reliable fit of its band gap decay with N. For comparison, we also calculated the band gap values for the ribbons with the single hydrogen at the edges (GNR-H) in its lowest energy antiferromagnetic spin-unrestiected [U] state.[1−4] In the [U] state GNR-H_2 ribbons have a 0.5 eV larger gap than GNR-H, while fluorination places GNR-F_2 band gaps on top of the GNR-H curve. Therefore we establish that the saturation of the zigzag GNR edge carbons leads to ribbons which also develop spin-polarized edges, just like zigzag ribbons with only sp^2 carbons.[1] Yet in contrast to GNR-H ribbons, such polarization only develops for GNR-H_2 ribbons that are larger than a certain width N.

To compare the relative stability of the [R] and [U] spin states, in Figure 3 we plot the formation energy of the ribbons. From the figure it becomes apparent why the [U] state appears only at $N = 6$: this is the narrowest ribbon width for which such a state is more energetically stable than [R]. Furthermore, all formation energies saturate with the width, indicating that the addition of extra carbons in the middle of the ribbon has a diminising effect on the edge stability. For the largest

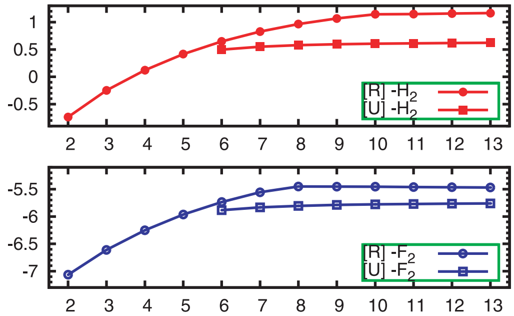

Figure 3. Formation energies of GNR-H_2 and GNR-F_2 as a function of *N*, in eV per unit cell (2 edge carbons). Graphene and H_2 or F_2 molecules are taken as the reference for the zero formation energies.

GNR-H_2 ribbon considered here ($N = 13$), the [U] state is more stable than [R] by 0.54 eV, while for GNR-F_2 at the same *N* the difference is smaller, 0.29 eV.

The band structures of GNR-H_2 and GNR-F_2 in the [R] state are given in Figure 4, while the band structure of the α-spin of GNR-H_2 in the [U] state is given in Figure 5a. The band structure for the β-spin is identical (although spatially different), and is not shown. In all these examples $N = 6$, corresponding to 10 sp^2 carbons per unit cell. The resulting 10 π bands visibly cluster in the band structure near the Π point. The narrowest separation between the highest occupied crystalline orbital (HOCO) and the lowest unoccupied crystalline orbital (LUCO) occurs near the Γ point, where the dispersion among the π bands is the largest. In all cases the HOCO has a maximum that is not at the Γ point, making the overall band gap of indirect character. In the [R] state of GNR-F_2 this HOCO maximum is more pronounced than in GNR-H_2, yielding larger differences between its direct and indirect gaps, and causing an earlier onset of metallicity in GNR-F_2 with respect to *N*. We also plot in the same figures the projected densities of states for the p_z orbitals of the two outer sp^2 carbons, p_z orbitals of the remaining sp_2 carbons, and all orbitals of the H or F atoms. In the orientation adopted here, the p_z orbitals are those orthogonal to the ribbon plane. In both [R] and [U] spin states the outer sp^2 carbons contribute significantly to the electronic bands near the gap, and the magnified densities of states near the gap highlight this observation (see the insets in Figures 4 and 5a). The p_z orbitals of the outer sp^2 carbons have the same weight in the states near the gap as the p_z orbitals of all the remaining sp^2 carbons. In contrast, in the other π bands the relative weight of the p_z orbitals of the two outer sp^2 carbons is noticably smaller. To further investigate the nature of the states near the gap, in Figure 5b we plot the frontier HOCO and LUCO orbitals for GNR-H_2 in the two spin states at the Γ point. The pictures reveal dramatic differences between these electronic configurations. In the [U] state the α-spin HOCO is on one edge of the ribbon, while α-spin LUCO is on the other, just like in the ribbons with sp^2 edges.[1−4] Naturally, for the β-spin the picture is reversed (not shown). Table 1 contains the ($\alpha - \beta$) spin density differences for GNR-H_2 and GNR-H. One can see that in GNR-H_2 the spin polarization wave exhibits a slower decay into the middle of the ribbon than in the

TABLE 1. (α-β) Spin Density Differences for GNR-H_2 and GNR-H Ribbons with *N* = 12

atom	GNR-H_2	GNR-H
H	0.071	−0.020
C_1	−0.137	0.471
C_2	0.576	−0.266
C_3	−0.328	0.230
C_4	0.422	−0.162
C_5	−0.262	0.136
C_6	0.272	−0.110
C_7	−0.185	0.096
C_8	0.183	−0.084
C_9	−0.139	0.077
C_{10}	0.137	−0.071
C_{11}	−0.119	0.068
C_{12}	0.118	−0.066

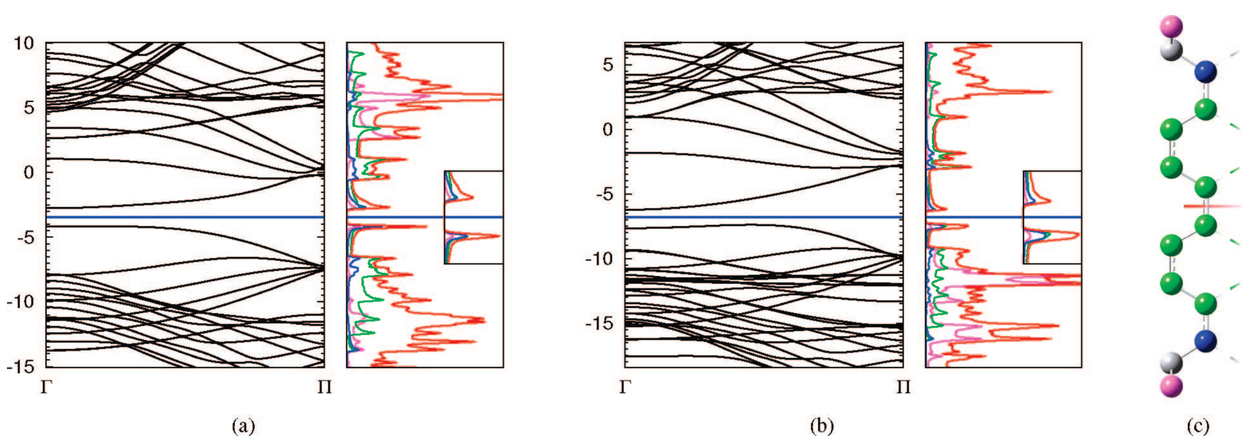

Figure 4. The PBEh [R] spin state band structures and density of states for (a) GNR-H_2 and (b) GNR-F_2 ribbons with *N* = 6 (the width of ~11 Å). The vertical axis is in eV. The total density of states (DOSes) is shown in red. Projected densities of states are colored according to structure (c) specifically, the p_z orbitals of the two outer sp^2 carbons are shown in blue, p_z orbitals of the remaining sp^2 carbons in the middle are shown in green, and all orbitals of the substituent (H or F) are shown in magenta. The insets in both DOSes show the magnified region near the gap, highlighting the large contribution of the outer (blue) sp^2 carbons.

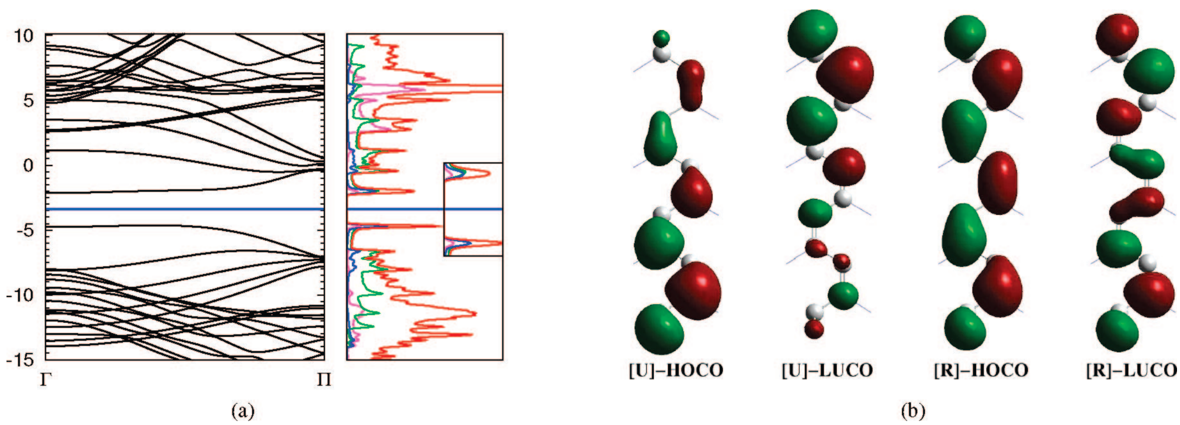

Figure 5. (a) The PBEh [U] spin state α-spin band structure and density of states for GNR-H_2 with $N = 6$ (the width of ~11 Å). The vertical axis is in eV. The total and projected densities of states are colored according to Figure 4c. (b) HOCO and LUCO orbitals for [U] and [R] spin states of GNR-H_2 with $N = 6$ (isovalue of 0.023). Note that the orbital vizualization software does not take into account the periodicity of the system, and therefore the orbitals do not appear symmetric with respect to the symmetry planes that exist along the vertically oriented carbon−carbon bonds.

case of GNR-H from ref 1 In contrast to the [U] state, in the [R] state HOCO and LUCO orbitals largely correspond to the bonding and antibonding combinations of the p_z orbitals of the outer sp^2 carbons, partially mediated by the other sp^2 carbons in the middle of the ribbon (Figure 5b). For the [R] state, as the ribbon width increases, the bonding–antibonding coupling between the edges decreases, and the HOCO and LUCO start to overlap in the energy spectrum. In the [U] state the ribbon width has a lesser effect on the nature of the localized edge states, and therefore the gap in this state is only slowly decaying. Because of the large contributions from the outer sp^2 carbons to the bands near the gap, the edge groups have a substantial effect on the absolute positions of both HOCO and LUCO levels. Specifically, in Figure 4a,b we observe that compared to GNR-H_2, in GNR-F_2 both HOCO and LUCO are shifted downward by about ~3 eV, and the same observation also applies for the [U] state (not shown). This is the trend that is found for all N's, and is caused by the high electronegativity of fluorine.

Figure 6 indicates carbon−carbon bond distances across the ribbon, starting from the edge. Irrespective of the edge substituent, the C_1—C_2 bond between the sp^3 and the sp^2 carbons is near the single C—C bond values, and is gradually decreasing with N. The next C_2—C_3 bond between the two outer sp^2 carbons starts out being of significant double bond character (low N's in the [R] state), with the gradual shift toward the conjugated C—C bond values similar to those found in the infinite graphene sheet (experimental value of 1.421 Å). Furthermore, the [R] state C_2—C_3 bond values make a jump toward the graphitic value at the N where the indirect gap becomes zero, while in the [U] state C_2—C_3 is close to the graphitic value already at $N = 6$ (where the [U] state becomes stable). In the [R] state the subsequent bonds (C_3—C_4, C_4—C_5, and C_5—C_6) alternate between single and double character, and approach the conjugated bond length value with increasing N. The same bonds in the [U] state exibit somewhat less pronounced alternation. Overall the [R] bond distances are most noticeably different from the corresponding [U] values for bonds closest to the double bond character, specifically, C_2—C_3 and C_4—C_5, with the difference for the former being the largest, on the order of 0.02 Å. Also noteworthy is a rather abrupt shift of these double bond-like distances for the [R] state toward the [U] state bond lengths (and graphitic value of 1.421 Å) right at the point where the [R] state band gap becomes zero. In comparison, GNR-H with all sp^2 carbons[1] in their lowest energy spin state [U] exhibit a much smaller modulation of carbon−carbon bonds. Their C_1—C_2 bond lengths are within the range of 1.404–1.407 Å, while the C_2—C_3 bond lengths are within the

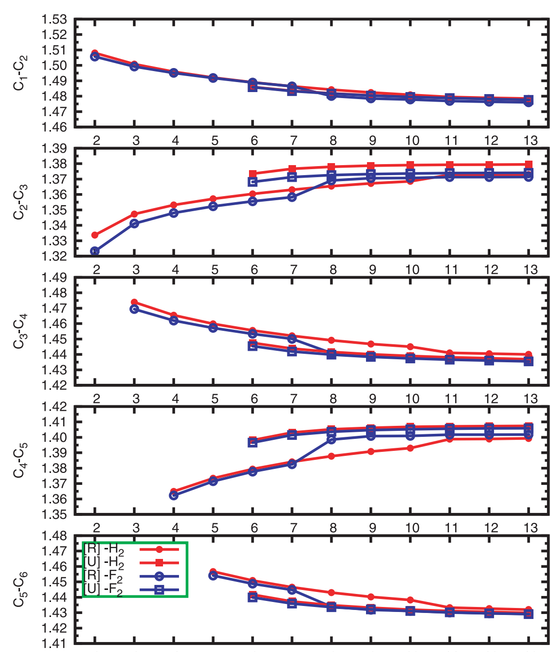

Figure 6. C—C bond length values (in Å) across CNR-H_2 and CNR-F_2, moving away from the edge as a function of N. From top to bottom, C_1—C_2, C_2—C_3, C_3—C_4, C_4—C_5, C_5—C_6 distances are given, see Figure 1 for atomic numbering.

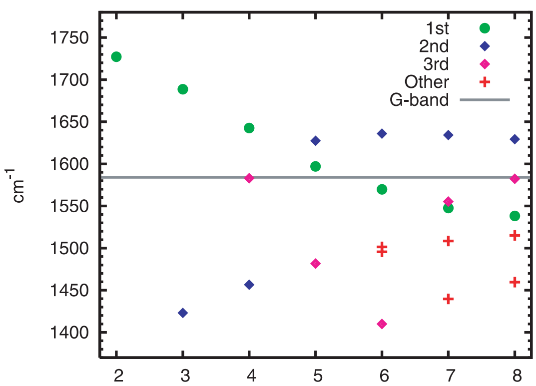

Figure 7. Raman active frequencies for GNR-H_2 with N = 2−8. The deuterium mass of 2 au is used for the H atom. The band of highest intensity (first), as well as second and third most intense bands are indicated by the corresponding symbols. The calculated graphene G-band is at 1584 cm^{-1}.

range of 1.458–1.439 Å (N = 2−13). All the other bonds are close to the graphitic value of 1.421 Å. Thus in sharp contrast to GNR-H_2, in GNR-H no carbon−carbon bonds are ever similar to double bonds.

Because in narrower ribbons the [R] state is the lowest in energy and has a very distinct bond alternation pattern, this state was the main focus of the Raman spectra calculations. The positions of Raman peaks for GNR-H_2 are given in Figure 7. For clarity of analysis, we used deuterium masses for H, since otherwise the H—C—H scissor mode (~1400 cm^{-1}) is significantly coupled with the in-plane vibrations of sp^2 carbons and would complicate the analysis. For comparison, we indicate in Figure 7 the position of the single Raman active frequency in a perfect graphene sheet (G-band)[28] calculated with similar parameters. The highest intensity Raman band in these ribbons is in the 1350–1750 cm^{-1} range corresponding to the in-plane sp^2 carbon vibrations, and decreases monotonically with increasing N. At N = 6 this band becomes lower in frequency than the G-band of graphene. However, even in structures where the highest intensity band is below the graphene G-band, there is still a peak of significant intensity above the G-band. This blue-shifted band is due to the significant double bond nature of the C_2—C_3 carbon bonds near the edges. For comparison, the frequencies of the [U] state of GNR-H_2 and GNR-H with N = 7 were also computed. In the [R] state of GNR-H_2 with N = 7 the highest carbon−carbon Raman active band is blue-shifted by 50 cm^{-1} with respect to the calculated G-band of graphene, while in the [U] state it is blue-shifted by only 26 cm^{-1} with respect to graphene. In contrast, in GNR-H a red shift is obtained, by 10 cm^{-1}, which is yet another indication of the lack of any bonds in GNR-H that would be close to double bond character. In other ribbon types the shift of the graphene G-band-like modes is also to the red.[29] As determined from the band structures, in the [R] state the opposite edges are strongly coupled *via* the HOCO−LUCO orbitals. This causes extensive delocalization of those π electrons that contribute the most to the polarizability derivatives (bands near the band gap), yielding large Raman intensities of the blue-shifted vibrational modes for $N \geq 3$. An exception are ribbons with N = 2 which only have isolated double bonds. With such bonds the π electrons do not delocalize beyond the two carbons participating in the bond, yielding lower Raman intensities.

CONCLUSIONS

In summary, by utilizing first principles calculations we investigated novel zigzag carbon ribbons with the sp^3 carbons on the edge. Ribbons with two different edge substituents were considered, hydrogen (GNR-H_2) and fluorine (GNR-F_2). The lowest electronic state of such ribbons depends on the ribbon width, with the restricted spin solution [R] being the most stable for $N < 6$, while the unrestricted spin solution [U] is the most stable for $N \geq 6$. In the ribbons with $N < 6$ the [R] state band gap lies in a wide range of 2–7 eV. The [U] state band gaps vary less and are within the range of 1−2.5 eV for ribbons with N = 6−13. Furthermore, in GNR-F_2 the HOCO and LUCO are shifted downward by ~3 eV compared to GNR-H_2, indicating the possibility to tune the absolute electronic band positions by varying the substituents. Compared to zigzag GNR with a single edge group such as GNR-H where the antiferfomagentically coupled edge states are already present in the narrowest ribbon with N = 2,[1] in the ribbons studied here such edge states only appear at $N \geq 6$. The calculated Raman spectra for narrower GNR-H_2 indicate the shift of the G-band like vibrations toward higher frequencies owing to the single-double carbon−carbon bond alternation. This shift diminishes with the ribbon width N and is smaller in the [U] state than in the [R] state. The distinct positions of the blue-shifted Raman peaks could offer a way for experimental identification of ribbons with the sp^3 edge carbons irrespective of the atomic environment into which these ribbons could be embedded.

METHODS

The bulk of calculations was carried out with the Gaussian 03 suite of programs[30] using the periodic boundary conditions implementation of Kudin and Scuseria.[22] Both gradient corrected and hybrid density functional methods,[23] specifically, PBE[24] and the hybrid PBEh (aka PBE0 and PBE1PBE)[25] functionals, respectively, were tested. Because of higher consistency of the PBEh results this functional has been used for all production calculations. Two basis sets of double-ζ quality were tested, 3-21G and 6-31G*. We found that the results for the 6-31G* basis were very similar to the 3-21G basis, and therefore we used the latter throughout. A uniform grid with 64 k points in the Brillouin zone was utilized with both functionals, with 29 real space cells used to compute the exact exchange integrals in the case of the PBEh functional. The structures were fully optimized with the periodic redundant coordinate optimization method[31] and visualized with the help of GaussView.[32] The orbital plots were also generated with this program.

Finally, the Raman spectra of GNR-H_2 were computed with the plane-wave approach utilizing the PBE functional[24] and norm-conserving pseudopotentials[33] implemented in the Quantum Espresso (QE) package.[34] Here, the 3D supercell calculations were carried out with 8 k points along the ribbon and large spacing in the other two directions. The periodic direction of the ribbons was optimized *via* the variable cell runs,[35] using cut-offs of 95 and 380 Ryd, respectively, with the modified kinetic energy functional.[36] Then, atomic positions were reoptimized with the fixed cell calculations utilizing lower 80 Ryd wave function and 320 Ryd charge density cutoffs. All these steps were necessary to ensure that the frequencies are evaluated at the energy minimum of the computational approach chosen for normal mode calculations. The Raman frequency calculations were carried out with the same fixed cell parameters by the phonon module of QE, where both frequencies[37] and Raman intensities[38] are computed *via* efficient analytic procedures. The graphene calculations were done with a 2-carbon hexagonal unit cell and an 8 × 8 grid of k points.

Acknowledgment. Financial support from the National Science Foundation NIRT under Grant No. CMS-0609049 is greatly appreciated. A computer time grant from the TIGRESS High Performance Computing Center at Princeton University is also acknowledged. The author is grateful to R. Car and I. A. Aksay for helpful discussions.

Supporting Information Available: Comparison of PBE and PBEh band gaps and PBEh optimized coordinates for GNR-H_2 and GNR-F_2 ribbons. This material is available free of charge *via* the Internet at http://pubs.acs.org.

REFERENCES AND NOTES

1. Fujita, M.; Wakabayashi, K.; Nakada, K.; Kusakabe, K. J. Peculiar Localized State at Zigzag Graphite Edge. *J. Phys. Soc. Jpn.* **1996**, *65*, 1920–1923.
2. Nakada, K.; Fujita, M.; Dresselhaus, G.; Dresselhaus, M. S. Edge State in Graphene Ribbons: Nanometer Size Effect and Edge Shape Dependence. *Phys. Rev. B* **1996**, *54*, 17954–17961.
3. Fujita, M.; Igami, M.; Nakada, K. Lattice Distortion in Nanographite Ribbons. *J. Phys. Soc. Jpn.* **1997**, *66*, 1864–1867.
4. (a) Miyamoto, Y.; Nakada, K.; Fujita, M. First-Principles Study of Edge States of H-Terminated Graphitic Ribbons. *Phys. Rev. B* **1999**, *59*, 9858–9861. (b) Miyamoto, Y.; Nakada, K.; Fujita, M. First-Principles Study of Edge States of H-Terminated Graphitic Ribbons. *Phys. Rev. B* **1999**, *60*, 16211.
5. Son, Y.-W.; Cohen, M. L.; Louie, S. G. Half-Metallic Graphene Nanoribbons. *Nature* **2006**, *444*, 347–349.
6. Hod, O.; Barone, V.; Peralta, J. E.; Scuseria, G. E. Enhanced Half-Metallicity in Edge-Oxidized Zigzag Graphene Nanoribbons. *Nano Lett.* **2007**, *7*, 2295–2299.
7. Gunlycke, D.; Li, J.; Mintmire, J. W.; White, C. T. Altering Low-Bias Transport in Zigzag-Edge Graphene Nanostrips With Edge Chemistry. *Appl. Phys. Lett.* **2007**, *91*. No. 112108.
8. Gunlycke, D.; Areshkin, D. A.; Li, J. W.; Mintmire, J. W.; White, C. T. Graphene Nanostrip Digital Memory Device. *Nano Lett.* **2007**, *7*, 3608–3611.
9. Rudberg, E.; Salek, P.; Luo, Y. Nonlocal Exchange Interaction Removes Half-Metallicity in Graphene Nanoribbons. *Nano Lett.* **2007**, *7*, 2211–2213.
10. Wang, Z. F.; Li, Q.; Zheng, H.; Ren, H.; Su, H. B.; Shi, Q. W.; Chen, J. Tuning the Electronic Structure of Graphene Nanoribbons Through Chemical Edge Modification: A Theoretical Study. *Phys. Rev. B* **2007**, *75*. No. 113406.
11. Jiang, D. E.; Sumpter, B. G.; Dai, S. First Principles Study of Magnetism in Nanographenes. *J. Chem. Phys.* **2007**, *127*. No. 124703.
12. Hod, O.; Peralta, J. E.; Scuseria, G. E. Edge Effects in Finite Elongated Graphene Nanoribbons. *Phys. Rev. B* **2007**, *76*. No. 233401.
13. Hod, O.; Barone, V.; Scuseria, G. E. Half-Metallic Graphene Nanodots. *Phys. Rev. B* **2008**, *77*. No. 035411.
14. Novoselov, K. S.; Geim, A. K.; Morozov, S. V.; Jiang, D.; Zhang, Y.; Dubonos, S. V.; Grigorieva, I. V.; Firsov, A. A. Electric Field Effect in Atomically Thin Carbon Films. *Science* **2004**, *306*, 666–669.
15. Zhang, Y.; Tan, Y.-W.; Stormer, H. L.; Kim, P. L. Experimental Observation of the Quantum Hall Effect and Berry's Phase in Graphene. *Nature* **2005**, *438*, 201–204.
16. Berger, C.; Song, Z.; Li, X.; Wu, X.; Brown, N.; Naud, C.; Mayou, D.; Li, T.; Hass, J.; Marchenkov, A. N.; Conrad, E. H.; First, P. N.; de Heer, W. A. Electronic Confinement and Coherence in Patterned Epitaxial Graphene. *Science* **2006**, *312*, 1191–1196.
17. Novoselov, K. S.; Jiang, Z.; Zhang, Y.; Morozov, S. V.; Stormer, H. L.; Zeitler, U.; Maan, J. C.; Boebinger, G. S.; Kim, P.; Geim, A. K. Room-Temperature Quantum Hall Effect in Graphene. *Science* **2007**, *315*, 1379.
18. Han, M. Y.; Ozyilmaz, B.; Zhang, Y.; Kim, P. Energy Band-Gap Engineering of Graphene Nanoribbons. *Phys. Rev. Lett.* **2007**, *98*. No. 206805.
19. Barone, V.; Hod, O.; Scuseria, G. E. Electronic Structure and Stability of Semiconducting Graphene Nanoribbons. *Nano Lett.* **2006**, *6*, 2748–2754.
20. Son, Y.-W.; Cohen, M. L.; Louie, S. G. Energy Gaps in Graphene Nanoribbons. *Phys. Rev. Lett.* **2006**, *97*. No. 216803.
21. Kudin, K. N.; Ozbas, B.; Schniepp, H. C.; Prud'homme, R. K.; Aksay, I. A.; Car, R. Raman Spectra of Graphite Oxide and Functionalized Graphene Sheets. *Nano Lett.* **2008**, *8*, 36–41.
22. Kudin, K. N.; Scuseria, G. E. Linear-Scaling Density-Functional Theory With Gaussian Orbitals and Periodic Boundary Conditions: Efficient Evaluation of Energy and Forces *Via* the Fast Multipole Method. *Phys. Rev. B* **2000**, *61*, 16440–16453.
23. Kohn, W.; Sham, L. J. Self-Consistent Equations Including Exchange and Correlation Effects. *Phys. Rev.* **1965**, *140*, A1133–A1138.
24. (a) Perdew, J. P.; Burke, K.; Ernzerhof, M. Generalized Gradient Approximation Made Simple. *Phys. Rev. Lett.* **1996**, *77*, 3865–3868. (b) Perdew, J. P.; Burke, K.; Ernzerhof, M. Generalized Gradient Approximation Made Simple. *Phys. Rev. Lett.* **1997**, *78*, 1396.
25. Perdew, J. P.; Ernzerhof, M.; Burke, K. Rationale for Mixing Exact Exchange With Density Functional Approximations. *J. Chem. Phys.* **1997**, *105*, 9982–9985.
26. Kudin, K. N.; Scuseria, G. E.; Martin, R. L. Hybrid Density-Functional Theory and the Insulating Gap of UO_2. *Phys. Rev. Lett.* **2002**, *89*. No. 266402.
27. Hirata, S.; Torii, H.; Tasumi, M. Density-Functional Crystal Orbital Study on the Structures and Energetics of Polyacetylene Isomers. *Phys. Rev. B* **1998**, *57*, 11994–12001.
28. Tuinstra, R.; Koenig, J. L. Raman Spectrum of Graphite. *J. Chem. Phys.* **1970**, *53*, 1126–1130.
29. Zhou, J.; Dong, J. Vibrational Property and Raman Spectrum of Carbon Nanoribbon. *Appl. Phys. Lett.* **2007**, *91*. No. 173108.
30. Frisch, M. J.; Trucks, G. W.; Schlegel, H. B.; Scuseria, G. E.; Robb, M. A.; Cheeseman, J. R.; Montgomery, J. A., Jr.; Vreven, T.; Kudin, K. N.; Burant, J. C.; *et al. Gaussian 03,* revision C.02; Gaussian, Inc.: Wallingford, CT, 2004.
31. Kudin, K. N.; Scuseria, G. E.; Schlegel, H. B. A Redundant Internal Coordinate Algorithm for Optimization of Periodic Systems. *J. Chem. Phys.* **2001**, *114*, 2919.
32. Dennington, R., II; Keith, T.; Millam, J.; Eppinnett, K.; Hovell, W. L.; Gilliland, R. *GaussView,* version 3.09; Semichem, Inc.: Shawnee Mission, KS, 2003.
33. Hamann, D. R.; Schluter, M.; Chiang, C. Norm-Conserving Pseudopotentials. *Phys. Rev. Lett.* **1979**, *43*, 1494–1497.

34. http://www.quantum-espresso.org.
35. Wentzcovitch, R. M.; Martins, J. L.; Price, G. D. Ab Initio Molecular-Dynamics With Variable Cell Shape−Application to $MgSiO_3$. *Phys. Rev. Lett.* **1993**, *70*, 3947–3950.
36. Bernasconi, M.; Chiarotti, G. L.; Focher, P.; Scandolo, S.; Tosatti, E.; Parrinello, M. J. First-Principle Constant-Pressure Molecular Dynamics. *J. Phys. Chem. Solids* **1995**, *56*, 501–505.
37. Baroni, S.; de Gironcoli, S.; Dal Corso, A.; Giannozzi, P. Phonons and Related Crystal Properties From Density-Functional Perturbation Theory. *Rev. Mod. Phys.* **2001**, *73*, 515–562.
38. Lazzeri, M.; Mauri, F. First-Principles Calculation of Vibrational Raman Spectra in Large Systems: Signature of Small Rings in Crystalline SiO_2. *Phys. Rev. Lett.* **2003**, *90*. No. 036401.